J|A|C|S
ARTICLES
Published on Web 05/01/2007

NMR Spin State Exchange Spectroscopy Reveals Equilibrium of Two Distinct Conformations of Leucine Zipper GCN4 in Solution

Yaroslav Nikolaev[†] and Konstantin Pervushin*[,§,†]

Contribution from the Laboratory of Physical Chemistry, Swiss Federal Institute of Technology (ETH Zurich), CH-8093 Zurich, Switzerland

Received December 6, 2006; E-mail: kpervushin@ntu.edu.sg

Abstract: The resonance assignment, secondary structure, and dynamic properties of a stable noncoiled coil conformation of the dimerization domain from yeast transcription activation factor GCN4 (Leu zipper; LZ_{GCN4}) are presented. Introduced in this paper, a new line of fully optimized spin state exchange experiments, XYEX-TROSY, applied to $^{1}H^{N}$, ^{15}N and $^{1}H^{\alpha}$,$^{13}C^{\alpha}$ moieties, established that in broad range of pH and buffer conditions the classical LZ_{GCN4} coiled coil dimer is in a dynamic equilibrium with another distinct conformation (denoted here as x-form) and enabled complete assignment of the resonances stemming from the x-form. The LZ_{GCN4} x-form is generally less structured in comparison with the classical GCN4-p1 coiled coil, but still retains a structured α-helical central core. The implications for folding properties and biological significance are discussed.

Introduction

Leucine zippers are a protein dimerization domain occurring in many eukaryotic enhancer-type transcription factors, referred to as basic leucine zipper proteins (bZIP)[1] and basic helix−loop−helix leucine zipper proteins (b-HLH-LZ).[2] Leucine zipper transcription factors have evolved as regulators in many processes that are critical to the function of an organism, from cell metabolism and differentiation[3] to circadian rhythms,[4] memory,[5] and development of organs.[6] These factors are widespread among eukaryotes, with only human genome containing 56 genes encoding proteins with 53 unique bZIP motifs.[7,8]

Because of their simplicity and stability leucine zippers have been widely used as a model system for kinetic and thermodynamic studies of protein folding[9−13] and references therein. In brief, in the common neutral saline phosphate buffer solution folding of the GCN4-p1 peptide is enthalpy-driven and opposed by a loss of entropy.[11] Folding proceeds via one or more stable intermediate states where a "trigger sequence" is proposed to adopt a helical conformation in the individual monomers which might be essential for successful association[14,15] resulting in a coiled coil structure[16,17] with some local structural transitions in the folded protein.[18] GCN4-p1 exhibits a complex temperature unfolding reaction consisting of several stages[12] featuring various degrees of structural losses with increasing temperature. Intra- and interhelical salt bridges stabilize GCN4-p1 but are not critical for maintenance of its 3D fold[10,19,20] and do not accelerate the folding.[21] Intriguingly as low as 0.1 mM concentration of SDS can initiate dissociation of the homodimer while retaining the secondary structure of the individual helices,[22] apparently interfering with both electrostatic and hydrophobic stabilizing interactions.

§ Current Address: School of Biological Sciences, Nanyang Technological University, Nanyang Drive 60, Singapore 637551.
† Current address: Biozentrum of University Basel, Klinlegbergstrasse 70, CH-4056, Basel, Switzerland.

(1) Landschulz, W. H.; Johnson, P. F.; McKnight, S. L. *Science* **1988**, *240*, 1759−64.
(2) Murre, C.; McCaw, P. S.; Vaessin, H.; Caudy, M.; Jan, L. Y.; Jan, Y. N.; Cabrera, C. V.; Buskin, J. N.; Hauschka, S. D.; Lassar, A. B. *Cell* **1989**, *58*, 537−44.
(3) Darlington, G. J.; Wang, N.; Hanson, R. W. *Curr. Opin. Genet. Dev.* **1995**, *5*, 565−70.
(4) Yamaguchi, S.; Mitsui, S.; Yan, L.; Yagita, K.; Miyake, S.; Okamura, H. *Mol. Cell. Biol.* **2000**, *20*, 4773−81.
(5) Sanyal, S.; Sandstrom, D. J.; Hoeffer, C. A.; Ramaswami, M. *Nature* **2002**, *416*, 870−74.
(6) Eferl, R.; Sibilia, M.; Hilberg, F.; Fuchsbichler, A.; Kufferath, I.; Guertl, B.; Zenz, R.; Wagner, E. F.; Zatloukal, K. *J. Cell Biol.* **1999**, *145*, 1049−61.
(7) Tupler, R.; Perini, G.; Green, M. R. *Nature* **2001**, *409*, 832−33.
(8) Vinson, C.; Myakishev, M.; Acharya, A.; Mir, A. A.; Moll, J. R.; Bonovich, M. *Mol. Cell. Biol.* **2002**, *22*, 6321−35.
(9) Lovett, E. G.; D'Avignon, D. A.; Holtzer, M. E.; Braswell, E. H.; Zhu, D.; Holtzer, A. *Proc. Natl. Acad. Sci. U.S.A.* **1996**, *93*, 1781−85.
(10) Kammerer, R. A.; Jaravine, V. A.; Frank, S.; Schulthess, T.; Landwehr, R.; Lustig, A.; Garcia-Echeverria, C.; Alexandrescu, A. T.; Engel, J.; Steinmetz, M. O. *J. Biol. Chem.* **2001**, *276*, 13685−88.
(11) Bosshard, H. R.; Durr, E.; Hitz, T.; Jelesarov, I. *Biochemistry* **2001**, *40*, 3544−52.
(12) Dragan, A. I.; Privalov, P. L. *J. Mol. Biol.* **2002**, *321*, 891−908.
(13) Wang, T.; Lau, W. L.; DeGrado, W. F.; Gai, F. *Biophys. J.* **2005**, *89*, 4180−7.
(14) Kammerer, R. A.; Schulthess, T.; Landwehr, R.; Lustig, A.; Engel, J.; Aebi, U.; Steinmetz, M. O. *Proc. Natl. Acad. Sci. U.S.A.* **1998**, *95*, 13419−24.
(15) Frank, S.; Lustig, A.; Schulthess, T.; Engel, J.; Kammerer, R. A. *J. Biol. Chem.* **2000**, *275*, 11672−7.
(16) O'Shea, E. K.; Klemm, J. D.; Kim, P. S.; Alber, T. *Science* **1991**, *254*, 539−44.
(17) Saudek, V.; Pastore, A.; Morelli, M. A.; Frank, R.; Gausepohl, H.; Gibson, T. *Protein Eng.* **1991**, *4*, 519−29.
(18) Holtzer, M. E.; Bretthorst, G. L.; d'Avignon, D. A.; Angeletti, R. H.; Mints, L.; Holtzer, A. *Biophys. J.* **2001**, *80*, 939−51.
(19) Spek, E. J.; Bui, A. H.; Lu, M.; Kallenbach, N. R. *Protein Sci.* **1998**, *7*, 2431−7.
(20) Zeng, X.; Herndon, A. M.; Hu, J. C. *Proc. Natl. Acad. Sci. U.S.A.* **1997**, *94*, 3673−8.
(21) Ibarra-Molero, B.; Zitzewitz, J. A.; Matthews, C. R. *J. Mol. Biol.* **2004**, *336*, 989−96.

Although GCN4-p1 has been extensively studied by NMR,[9,10,17,18,23−25] to our knowledge all these studies were conducted at high protein concentrations between 1.4 mM to 6 mM and mainly at neutral pH. However even in the first structural NMR study[17] it was observed that a set of unidentified NMR resonances stemming from GCN4-p1 appears at lower protein concentration. This urged us to conduct an NMR-based structure determination at ca. 6−8 mM of GCN4-p1 where the equilibrium is strongly shifted toward the classical coiled coil state.[16]

Here we report our findings that at concentrations below 0.5 mM in acidic and up to neutral pH conditions in TRIS ([1,3-dihydroxy-2-(hydroxymethyl)propan-2-yl]azanium), NaPi, acetate, and HEPES (2-[4-(2-hydroxyethyl)piperazin-1-yl]ethanesulfonic acid) buffers a conventional coiled coil state of the LZ_{GCN4} is in dynamic equilibrium with a distinctively different conformational state of the same peptide. Moreover, at pH = 3.2 and peptide concentrations below 150 μM this conformation dominates the equilibrium. To characterize this dynamic equilibrium a novel pseudo-four-dimensional fully sensitivity enhanced spin-state exchange TROSY experiment was developed, together with its two-dimensional predecessors[26,27] providing evidence that the two conformation states of LZ_{GCN4} are exchanging with the rate of $16.98 \pm 0.96\ s^{-1}$, which coincides with the interconversion rate of two folded forms of GCN4-p1 found by $^{13}C^{\alpha}$ NMR[18] and is by 3 orders of magnitude slower than the main folding reaction of LZ.

Results

Sample Conditions and Assignment of NMR Resonances. To investigate conformational equilibrium in Leu-zipper dimerization domain a 36 residue uniformly ^{15}N, ^{13}C-labeled recombinant LZ_{GCN4} peptide was expressed in *E. coli* as a cleavable fusion with bacteriophage λ protein D bearing N-terminal $(His)_6$ tag. Except for the N-terminal Gly a complete assignment of $^{1}H^{N}$, $^{1}H^{\alpha}$, $^{1}H^{\beta}$, ^{15}N, $^{13}C'$, $^{13}C^{\alpha}$, and $^{13}C^{\beta}$ resonances of LZ_{GCN4} was obtained at the peptide concentration of 1 mM and pH 7.1 using standard NMR techniques confirming the assignment of ^{1}H and ^{13}C resonances reported earlier.[9,17] At lower peptide concentrations, a second distinct set of cross-peaks in [^{1}H, ^{15}N]-HSQC spectra (see Figure 1A) is evident, which we attributed to yet another, so far uncharacterized, conformation of LZ_{GCN4}. For the sake of convenience we dub this conformation of LZ_{GCN4} as "x-form" to distinguish it from the known coiled-coil conformation, designated here as "cc-form".

Analysis of the cc-form versus x-form population equilibrium based on [^{1}H, ^{15}N]-HSQC spectra revealed that the x-form dominates at low peptide concentrations in the acidic pH, reaching as high as 83% at 15 μM and pH 3.2 (Figure 2A). Intriguingly, the x-form is still detectable by NMR at neutral pH reaching 10% of the total population at the concentration of the peptide monomer of 250 μM and pH 5.5, slightly decreasing to 8% population at the concentration of 30 μM and pH 7.1 (Figure 2A). On the basis of these observations the conditions for more detailed NMR studies were chosen in such a way that both conformations are approximately equally populated (concentration of the peptide monomer of 250 μM and pH 3.2). At these conditions 3D HNCA, HNCACB, CBCA(CO)NH, HBHA(CO)HN, and ^{13}C, ^{15}N-resolved NOESY experiments were recorded. Despite the availability of assignment of the cc-form, these triple resonance experiments were proven not to be sufficient for unequivocally assigning all of the backbone resonances of the x-form. This problem has been pinpointed to the presence of conformational exchange between two forms with the characteristic exchange times coinciding with the magnetization transfer periods in triple resonance experiments resulting in an often intractable mixture of cross-peaks in the 2D [^{1}H, ^{15}N] strips taken along the ^{13}C dimension. This called for complementing the standard set of NMR experiments with an experiment selectively correlating resonances from two exchanging forms with highest sensitivity and without interference with other coherence transfer pathways.

Spin States Exchange Experiments with LZ. Figure 3 shows the pulse sequence for the pseudo-four-dimensional spin-state exchange XYEX-TROSY experiment, which is a fully sensitivity enhanced, transverse relaxation optimized NMR experiment, deployed here to unequivocally correlate $^{1}H^{N}$, ^{15}N, and $^{1}H^{\alpha}$, $^{13}C^{\alpha}$ cross-peaks stemming from two exchanging forms of LZ_{GCN4}. Mixing of the coherences in the transverse plane while preserving the individual spin-states enables implementation of the echo−anti-echo quadrature detection method[28] in all indirectly acquired spectral dimensions resulting in the fully sensitivity-enhanced 4(1)D experiment. The key feature of the proposed experiment is a convoluted evolution of the zero- and double-quantum coherencies originating from the exchanging conformations before they are mixed in the transverse plane and detected via the ST2-PT[29] or ZQ/DQ TROSY[30] schemes.

Figure 4A shows 2D [DQ/ZQ, $^{1}H^{N}$] strips taken at the corresponding ^{1}H and ^{15}N chemical shifts of the observed cross-peaks in the fingerprint [^{1}H, ^{15}N] TROSY spectra. With the use of XYEX-TROSY identification of the pairs of exchanging resonances stemming from the same amide group (or $^{1}H^{\alpha}-^{13}C^{\alpha}$ moieties, see Figure 4B) is straightforward and requires the presence of only one cross-peak usually of the most populated conformation. This is because all four chemical shifts required to link exchanging spin-systems can be inferred from the positions of a single exchange cross-peak in ZQ and DQ subspectra of the same XYEX-TROSY experiments. The opposite situation is encountered in the analysis of 3D ^{15}N or ^{13}C-resolved NOESY spectra,[31] where the presence of a pair of "forward" and "return" cross-peaks is mandatory to unequivocally link interacting spin systems.

For large proteins the DQ subspectrum of XYEX-TROSY might be significantly more sensitive comparing to the ZQ subspectrum due to the TROSY effect.[32] Even for 8.6 kDA LZ_{GCN4} dimer, a comparison between these two subspectra

(22) Meng, F. G.; Zeng, X. G.; Hong, Y. K.; Zhou, H. M. *Biochimie* **2001**, *83*, 953−56.
(23) Lumb, K. J.; Kim, P. S. *Science* **1995**, *268*, 436−9.
(24) Weiss, M. A.; Ellenberger, T.; Wobbe, C. R.; Lee, J. P.; Harrison, S. C.; Struhl, K. *Nature* **1990**, *347*, 575−8.
(25) Holtzer, M. E.; Lovett, E. G.; d'Avignon, D. A.; Holtzer, A. *Biophys. J.* **1997**, *73*, 1031−41.
(26) Wider, G.; Neri, D.; Wuthrich, K. *J. Biomol. NMR* **1991**, *1*, 93−98.
(27) Sprangers, R.; Gribun, A.; Hwang, P. M.; Houry, W. A.; Kay, L. E. *Proc. Natl. Acad. Sci. U.S.A.* **2005**, *102*, 16678−83.
(28) Kay, L. E.; Keifer, P.; Saarinen, T. *J. Am. Chem. Soc.* **1992**, *114*, 10663−5.
(29) Pervushin, K.; Wider, G.; Wuthrich, K. *J. Biomol. NMR* **1998**, *12*, 345−48.
(30) Pervushin, K.; Wider, G.; Riek, R.; Wuthrich, K. *Proc. Natl. Acad. Sci. U.S.A.* **1999**, *96*, 9607−12.
(31) Cavanagh, J.; Fairbrother, W. J.; Palmer, A. G.; Skelton, N. J. *Protein NMR Spectroscopy: Principles and Practice*; Academic Press: New York, 1996.
(32) Pervushin, K.; Riek, R.; Wider, G.; Wuthrich, K. *Proc. Natl. Acad. Sci. U.S.A.* **1997**, *94*, 12366−71.

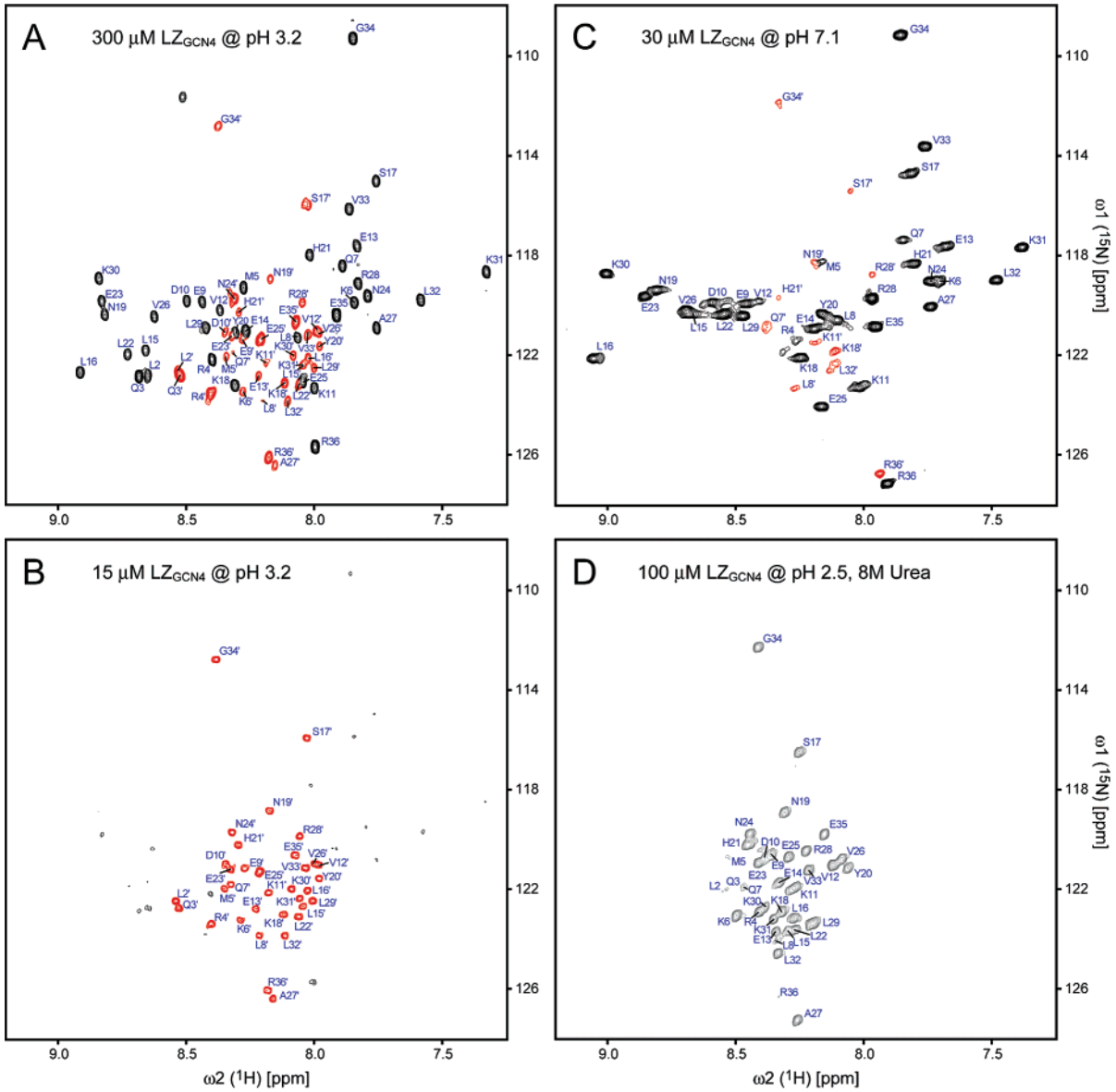

Figure 1. Equilibrium of two distinct LZ_{GCN4} conformations. [^{15}N-^{1}H]-HSQC NMR spectra of ^{15}N-^{13}C-labeled LZ_{GCN4} recorded at 37 °C and 600 MHz: (A) 300 μM and (B) 15 μM peptide (monomer concentrations) in 50 mM D_3-acetate, 40 mM KCl, 10% D_2O, pH 3.2; (C) 30 μM peptide in 20 mM D_{18}-HEPES, 80 mM KCl, 10% D_2O, pH 7.1; (D) 100 μM peptide in 8 M urea, pH 2.5. Assignment corresponds to $LZ_{cc-dimer}$ (black contours), LZ_{x-form} (red contours), $LZ_{unfold\ monomer}$ (gray contours, (D)).

(Figure 4) reveals reduced S/N in the ZQ subspectrum, with some exchange cross-peaks disappearing into the spectral noise. In this situation the only DQ subspectrum can be used to establish exchanging spin systems via search of forward and return cross-peak as it is in conventional 3D NOESY. Alternatively, ZQ evolution can be observed using the TROSY pathway in a separate experiment, which can be obtained from the one shown in Figure 3 by inverting the phase of the last ^{15}N 90° pulse.

Analysis of the [^{1}H, ^{15}N]-XYEX-TROSY strips along DQ and ZQ dimensions corresponding to the cross-peaks in [^{1}H, ^{15}N]-HSQC spectrum for the LZ_{GCN4} molecule yielded in assignment of all 35 pairs of the amino acid residues under exchange. [^{1}H, ^{15}N]-XYEX-TROSY strips correlating exchanging cross-peaks can also serve as an additional source of information to resolve resonances completely overlapping in the HSQC spectrum. We found that residues K31′/L15′, V12′/V26′, L2′/Q3′, and L22′/E25 exhibiting this kind of spectral degeneracy nonetheless can be assigned using the set of exchange peaks in the multiple-quantum dimension.

The [$^{1}H^{\alpha}$,$^{13}C^{\alpha}$]-XYEX-TROSY experiment showed slightly decreased S/N ratio in comparison with the [$^{1}H^{N}$,^{15}N]-XYEX-TROSY owing to partial dephasing of magnetization during all chemical shift evolution periods as well as the mixing period owing to the passive $^{1}J_{C\alpha C\beta}$ and $^{n}J_{H\alpha Hi}$ with $n > 2$ couplings. Analysis of the [$^{1}H^{\alpha}$,$^{13}C^{\alpha}$]-XYEX-TROSY spectra yielded resolved correlations of $^{13}C^{\alpha}$ resonances for 19 residues (with others being overlapped). As an alternative to the mixing of exchanging coherences in the transverse plane, we tested mixing in the longitudinal direction. ZEX-TROSY experiments (Supporting Information) developed to achieve this goal showed nonetheless a similar *S/N* ratio for the exchange cross-peaks, confirming the functionality of the proposed mixing strategy employed in XYEX-TROSY at least for LZ_{GCN4}.

Since the XYEX-TROSY series of experiments provides the maximal theoretically achievable sensitivity in the pseudo-4D

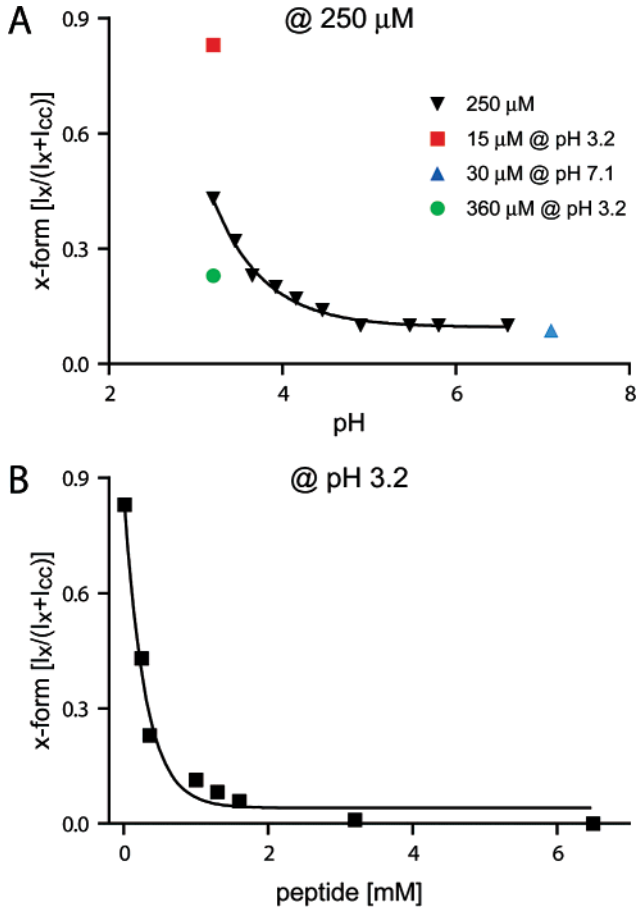

Figure 2. The pH (A) and concentration (B) dependences of LZ_{GCN4} x-form population. The x-form populations were determined from the relative volumes of [^{1}H-^{15}N]-HSQC peaks corresponding to each conformation: $I_X/(I_X + I_{CC})$ where I_X and I_{CC} refer to the intensities of peaks of the x-form and coiled coil, respectively. Peak intensities for calculations are taken as averages of 10 peaks for each conformation at each data point.

spectrum, it demonstrates practical advantages over the existing 3D versions developed earlier.[26,27,33] The maximum sensitivity requirement together with the higher resolution achieved in pseudo-4D spectra are especially important in studies of LZ_{GCN4} at low concentrations used to populate the x-form exhibiting significant spectral degeneracy. Although visible even for this small protein, the TROSY effect is of less importance for sensitivity improvement. Here the TROSY-based polarization transfer schemes were used as a convenient tool to preserve spin states during coherence transfers. Of course, for larger proteins the TROSY effect might become the most prominent source of sensitivity and resolution improvements.

To quantitatively characterize the exchange process under observation a two-dimensional version of the spin-state longitudinal exchange experiment[27] was employed (Figure 5), yielding an interconversion rate of 16.98 ± 0.96 (SE) s^{-1} for two forms of LZ_{GCN4}. This rate strongly coincides with the interconversion rate of two folded forms of GCN4-p1 found by $^{13}C^{\alpha}$ NMR[18] and, most intriguingly, is by 3 orders of magnitude slower than the main folding reaction of LZ_{GCN4}, as determined from the stopped-flow circular dichroism studies.[34]

(33) Farrow, N. A.; Zhang, O.; Forman-Kay, J. D.; Kay, L. E. *J. Biomol. NMR* **1994**, *4*, 727−34.
(34) Zitzewitz, J. A.; Bilsel, O.; Luo, J.; Jones, B. E.; Matthews, C. R. *Biochemistry* **1995**, *34*, 12812−9.

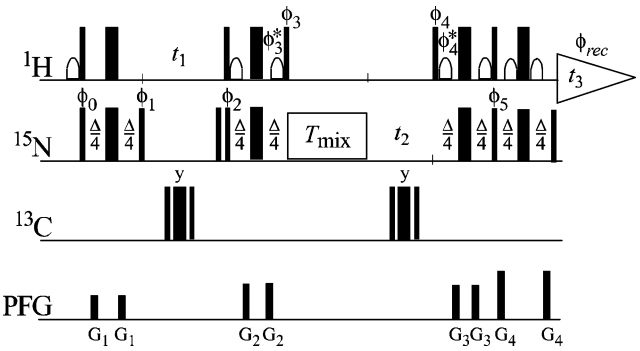

Figure 3. Scheme of 4(1)D XYEX-TROSY, pseudo-four-dimensional spin-state exchange TROSY experiment with mixing of spin coherencies in the transverse plane utilizing an entire steady-state Boltzmann thermal equilibrium magnetization and featuring sensitivity enhancement for the phase sensitive detection in all three spectral dimensions suitable for two coupled $^1/_2$ spin systems. Narrow and wide black bars indicate nonselective $\pi/2$ and π rf-pulses applied with the phase x unless indicated otherwise. Water saturation is minimized by returning the water magnetization to the $+z$-axis before data acquisition by the use of water selective 90° rf-pulses shown as open shapes on the ^{1}H channel. The time period Δ is set to $1/J_{HN}$ and is 5.78 ms for the backbone amide moieties. The ^{1}H spin-state selective ^{15}N coherences stemming from kinetically exchanging spin systems are mixed during a T_{mix} period using a planar mixing scheme IICT-4, which is a composite pulse sequence specifically designed for isotropic mixing purpose in TOCSY experiments (see Materials and Methods).[61] The IICT-4 scheme is RRRRRRRR with R = 38(0), 112.6(60.5), 205.9(68.6), 256.9(280.1), 101.9($\overline{5.2}$), $\overline{265}$.5(281.6), 242.6(72.6), 66.6(66.9), 44.9(0), where numbers represent rf-pulses with the corresponding flip angle and the rf-phase (in brackets), respectively, and $\underline{R}$ is phase inversion of R. In this case the durations and strengths of the pulsed magnetic field gradients (PFG) applied along the z-axis are selected as (G_1) 500 μs, 19 G/cm; (G_2) 500 μs, 15 G/cm; (G_3) 900 μs, 32 G/cm; (G_4) 1 ms, 50 G/cm. Two datasets, S_{ZQ+DQ} and S_{ZQ-DQ}, are acquired using the phases $\phi_0 = \{x, -x\}$; $\phi_1 = \{y, -y\}$; $\phi_2 = -x$; $\phi_3 = -y$; $\phi^*_3 = y$; $\phi_4 = y$; $\phi^*_4 = -y$; $\phi_5 = y$; $\phi_{rec} = \{-y, y\}$ for S_{ZQ+DQ} and $\phi_0 = \{-y, y\}$; $\phi_1 = \{x, -x\}$; $\phi_{rec} = \{x, -x\}$ for S_{ZQ-DQ}. For both S_{ZQ+DQ} and S_{ZQ-DQ} datasets the quadrature detection in t_1 and t_2 dimensions is achieved by the echo−anti-echo method.[28,64] For the dataset S_{ZQ+DQ} the anti-echo signal in t_1 dimension is obtained by inversion of the phases ϕ_2, ϕ_3, and ϕ^*_3, and the anti-echo signal in t_2 dimension is obtained by inversion of the phases ϕ_2, ϕ_3, ϕ^*_3, ϕ_4, ϕ^*_4, and ϕ_5. For the dataset S_{ZQ-DQ} the anti-echo signal in t_1 dimension is obtained by inversion of the phases ϕ_1, ϕ_2, ϕ_3, and ϕ^*_3, and the anti-echo signal in t_2 dimension is obtained by inversion of the phases ϕ_2, ϕ_3, ϕ^*_3, ϕ_4, ϕ^*_4, and ϕ_5. The processing of the datasets is described in Materials and Methods and the listings of pulse programs for Bruker Avance spectrometers are available in Supporting Information. The rf-pulses on the ^{1}H, ^{15}N, and ^{13}C nuclei are centered at 4.7, 118, and 110 ppm, respectively.

Secondary Structure of the x-Form. A complementary set of experiments (HNCA, HNCACB, CBCA(CO)NH, ^{1}H-^{15}N NOE) was carried out with LZ_{GCN4} in 8 M urea, yielding the assignment (Figure 1D) and dynamic characterization (Figure 6B) of the LZ_{GCN4} truly unfolded state. These data were used as a reference point to unequivocally exclude the possibility of the observed x-form species being unfolded LZ_{GCN4} monomer. Additionally, a set of HNCA, CBCA(CO)NH, and ^{1}H-^{15}N NOE experiments was recorded in the conditions of the x-form dominating the equilibrium (25 μM monomer concentration at pH 3.2). These spectra were used to obtain unbiased by exchange input data for characterization of secondary structure and dynamics of the x-form.

Secondary chemical shifts of the cc- and x-forms (Figure 6C-E) were calculated using the random coil chemical-shift values of the authentic LZ_{GCN4} sequence in 8 M urea. A comparison of secondary chemical shift data of the cc-form versus the x-form points out that the x-form is indeed considerably less structured. However, the appearance of the δC_α and δC_β plots

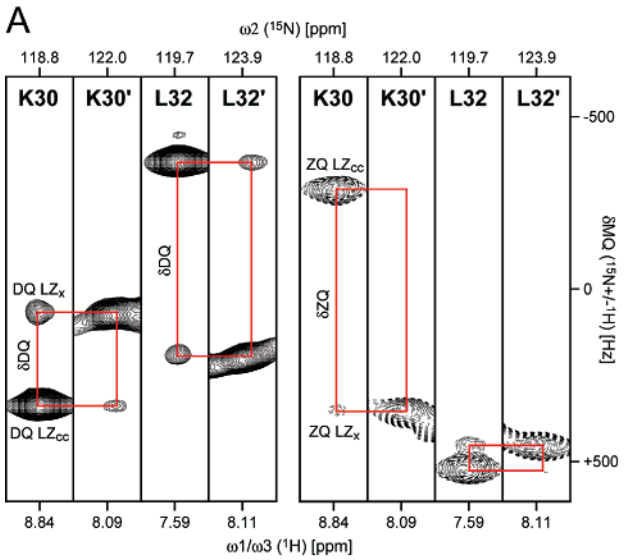

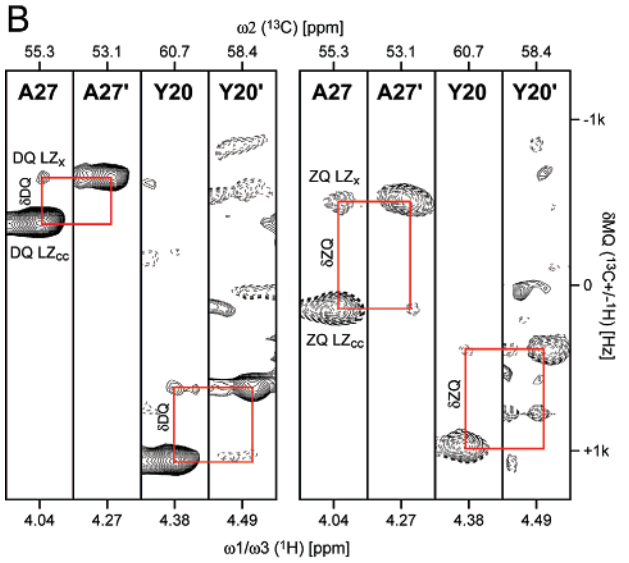

Figure 4. Correlation of exchanging conformations by XYEX-TROSY. Strip plots for K30, L32 (A) and A27, Y20 (B) residues from DQ and ZQ subspectra of the [$^1H^N$, ^{15}N]-XYEX-TROSY (A) and [$^1H^\alpha$, $^{13}C^\alpha$]-XYEX-TROSY (B) NMR experiments. Spectra recorded using 360 μM ^{15}N-^{13}C-labeled LZ_{GCN4}, at 37 °C and 600 MHz.

indicates the presence of residual α-helical structure. This residual alpha-helical propensity is mainly confined to two clusters around valine residues 12 and 26, localized in the "a" positions of leucine zipper heptad repeats[1] and contributing to the hydrophobic lock of the zipper structure. The same Val12 and Val26 residues also show the strongest helical secondary C_α shifts in the coiled coil conformation.

The observation of the steady-state heteronuclear ^1H-^{15}N NOEs (Figure 6B) indicates that the x-form is significantly less structured when compared to the LZ_{GCN4} coiled coil dimer. Nevertheless, it still retains a structural core localized to the residues Lys11 to Leu29 representing two LZ heptad repeats out of four total. At the same time the residues at the N- and C-termini exhibit strongly negative HNOE values, which is again indicative of low-spatial restriction and enhanced mobility in a nanosecond time scale. Noteworthy, x-form looks considerably more restrained in terms of the dynamics than the unfolded

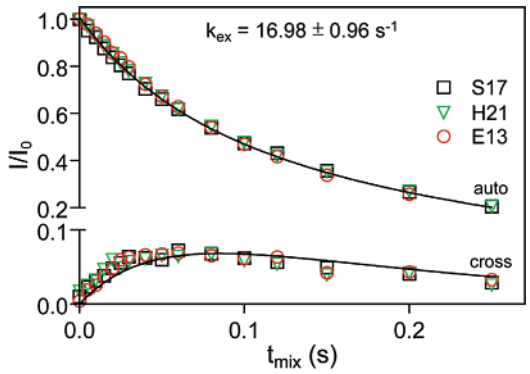

Figure 5. Characterization of exchange process. Longitudinal (H_zN_z) exchange spectroscopy recorded for LZ_{GCN4} at 37 °C. The decay of autopeaks and buildup of cross-peaks is illustrated, where I/I_0 is the intensity of a given correlation normalized to the maximum intensity of the appropriate autopeak at the zero mixing time. Experimental data points correspond to the residues Ser17 (squares), Glu13 (circles), and His21 (triangles). The solid lines correspond to the best fits of the data (all six curves fitted simultaneously) as described in Sprangers et. al.[27]

monomer. This difference shall be much more prominent if one considers the effect of 8 M urea on the viscosity of solution. Additionally the observed regular patterns of $^1H^N/^1H^N$ $d_{NN}(i,i+1)$ NOEs confined to the same central region of the x-form (e.g., residues 11−13, 15−16, 19−22, and 24−26) as well as $d_{\beta N}(i,i+1)$ NOEs (residues 9−13 and 15−29) (data not shown) are consistent with the presence of α-helical structure,[35] albeit this should be interpreted with caution since unstructured peptides may also show sequential amide protons contact patterns. The detailed structure determination of the x-form is delegated to future work.

Discussion

NMR studies of LZ_{GCN4} at low concentrations and broad range of pH and buffer conditions, revealed the presence of a second, thermodynamically stable conformation, designated as the x-form, which so far has escaped structural characterization. Introduced in this paper, a new line of fully optimized spin state exchange experiments, XYEX-TROSY, applied to $^1H^N$, ^{15}N and $^1H^\alpha$, $^{13}C^\alpha$ moieties, established that the x-form is in a dynamic equilibrium with the classical coiled coil conformation of the LZ_{GCN4} and enabled complete assignment of the resonances stemming from the x-form. This equilibrium is evident not only in ^{15}N-labeled recombinant LZ_{GCN4}, but also in a chemically synthesized LZ_{GCN4} peptide (e.g., as $^1H^N/^1H^N$ cross-peaks in [^1H, ^1H]-TOCSY spectra), as well as in the full-length recombinant bZIP motif of GCN4. This compels us to attribute this equilibrium to intrinsic properties of the LZ_{GCN4} sequence.

In fact, concentration dependent conformational equilibrium of the classical coiled coil LZ_{GCN4} conformation with some other species was noted as early as the first homonuclear NMR structural study of GCN4-p1,[17] and later in the ^{13}C studies of GCN4-p1[18] and its GCN4-lzK modification.[9] However, in all cases the x-form was considered as being either unfolded monomer or an intractable ensemble of (artificial) folding intermediates and no further investigation or characterization of the detected species was done.

The LZ_{GCN4} x-form appears to be a stable folding intermediate that is considerably populated under a wide range of conditions.

(35) Wuthrich, K. *NMR of Proteins and Nucleic Acids*; Wiley: New York, 1986.

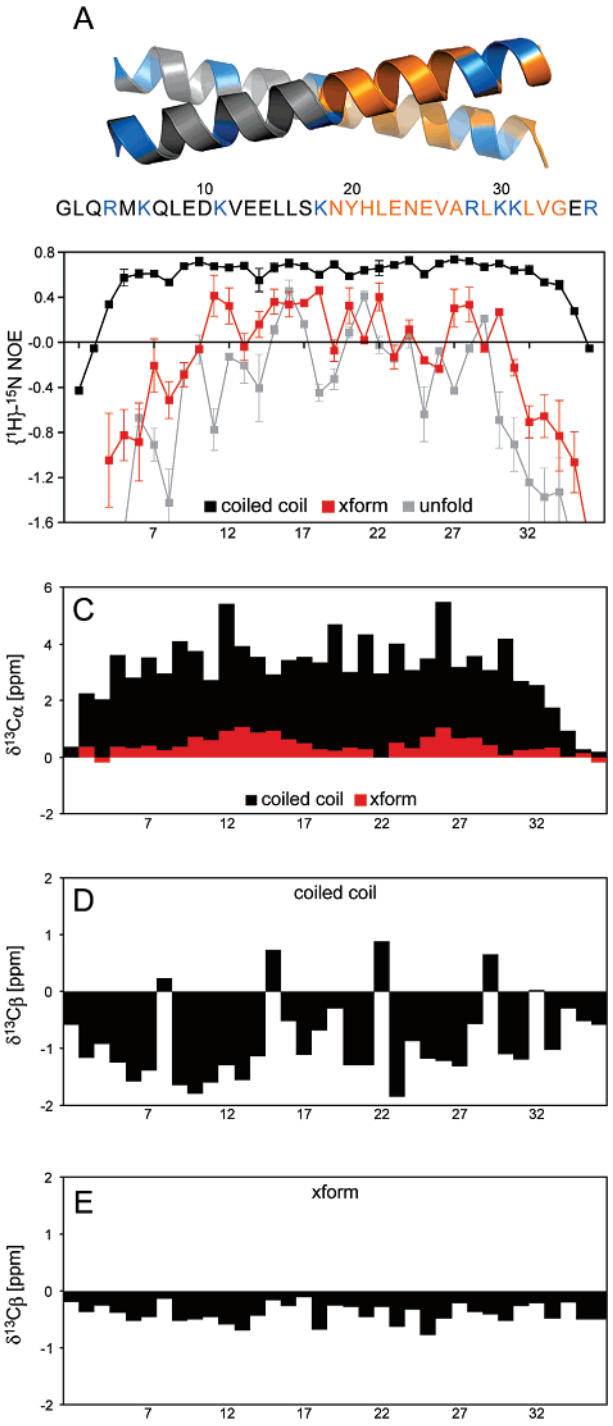

Figure 6. Preliminary structural characterization of the LZ_{GCN4} x-form. (A) 3D structure of the 31 residue LZ_{GCN4} coiled coil dimer (pdb code 2zta[16]) aligned with the sequence of the LZ_{GCN4} peptide used in the current study. The triggering sequence[14] is marked with orange; basic amino acid residues, capable of generating side-chain repulsive interactions in acidic pH, are marked with blue. (B) Heteronuclear [^{1}H-^{15}N] NOEs of cc-form (black squares), x-form (red squares), and urea-unfolded form (gray squares) measured respectively at 360 μM, 25 μM, and 100 μM of LZ_{GCN4} at pH 3.2 and 37 °C. Secondary chemical shifts for $C^{\alpha}_{cc-form}$ (black bars) and C^{α}_{x-form} (red bars) (C), $C^{\beta}_{cc-form}$ (D), and C^{β}_{x-form} (E), resonances calculated relative to the random coil chemical-shift values of the urea-unfolded form.

Notwithstanding its generally less structured appearance in comparison with the classical GCN4-p1 coiled coil, this conformation still retains a structured α-helical central core (Results section and Figure 6). Consistent with the possibility of dimeric nature of the x-form are observations that while GCN4-p11-33 (fragment of GCN4-p1 comprising residues 11 to 33) is monomeric, slightly longer GCN4-p8-33 is predominantly dimeric.[36] Data from other research groups indicate that LZ_{GCN4} folding intermediate contains a considerable amount of preformed helical structure already at the point when the collision of monomer chains occurs.[14,37−39] Experimental data of Zitzewitz and co-workers,[38] utilizing the φ-analysis[40] to assess the effect of mutations on the structure of the transition state, indicates that about one-third of the LZ_{GCN4} molecule (approximately three turns of the α-helix) may be structured in the transition state. Their data provide an evidence for the role of a preformed helix in a transition state leading to the natively folded dimer.

Interestingly, C_β secondary chemical shifts of all four Leu residues at the coiled coil d-positions forming the hydrophobic interface of the dimer, turn out to be positive in contrary to δC_β of all other residues (Figure 6D). This indicates that the location of C_βs proximally to the dimer interface makes them quite sensitive to the changes in the hydrophobic interactions. In contrast, the residues at the a-positions of the coiled coil, which are also involved in the hydrophobic interface, do not show the same effect. Elimination of denoted positive C_β secondary chemical shifts of Leu residues at the d-positions of the x-form (Figure 6E) comparing to the coiled coil structure shows that there are substantial changes in the knobs-into-holes packing characteristic to the coiled coil dimer, implying monomeric structure of the x-form. This assumption goes in line with strong concentration dependence of the x-form versus cc-form populations. However, currently we have insufficient data to make unequivocal conclusions about the monomeric versus dimeric nature of the x-form, and its exact 3D arrangement still awaits characterization.

Kammerer et al.[14] has reported the trigger sequence (autonomous folding unit) essential for oligomerization of dimeric coiled coils. In the GCN4 transcription factor this sequence is represented by third and fourth heptad repeats of the leucine zipper domain. From the current set of NMR data on the x-form including steady-state heteronuclear ^{1}H-^{15}N NOEs, $^{13}C_\alpha$ and $^{13}C_\beta$ secondary chemical shifts (Figure 6), and patterns of sequential NOE connectivities (Results section), the presence of the triggering sequence with higher α-helical content proposed by Kammerer and colleagues is not evident. It rather appears that there are two triggering sites localized proximally to the valine residues in the zipper "a" positions 12 and 26 (at the boundaries of first-second and third-fourth heptad repeats). Alternatively current NMR data would indicate that x-form represents a stable folding intermediate at the native site of the folding barrier, while the triggering sequence of more structured C-terminal heptads exists at the level of a LZ_{GCN4} random coil monomer before the chain collision event.

Additionally, it was shown that α-helical content in the peptide corresponding to this trigger sequence strongly depends on the pH, suggesting existence of repulsive interactions between

(36) Lumb, K. J.; Carr, C. M.; Kim, P. S. *Biochemistry* **1994**, *33*, 7361−7.
(37) Myers, J. K.; Oas, T. G. *J. Mol. Biol.* **1999**, *289*, 205−9.
(38) Zitzewitz, J. A.; Ibarra-Molero, B.; Fishel, D. R.; Terry, K. L.; Matthews, C. R. *J. Mol. Biol.* **2000**, *296*, 1105−16.
(39) Moran, L. B.; Schneider, J. P.; Kentsis, A.; Reddy, G. A.; Sosnick, T. R. *Proc. Natl. Acad. Sci. U.S.A.* **1999**, *96*, 10699−704.
(40) Serrano, L.; Matouschek, A.; Fersht, A. R. *J. Mol. Biol.* **1992**, *224*, 805−18.

side chains of basic amino acid residues, and indicating the importance of electrostatic interactions for the overall helix stability.[14] These data can be used to indirectly interpret the pH dependence of the x-form versus the cc-form at the equilibrium. The GCN4p16-31 peptide used by Kammerer and colleagues incorporates just third and fourth heptad repeats of GCN4, and contains only 3 basic amino acid residues total (corresponding to R28, K30, K31 in LZ_{GCN4}) within these two heptad repeats. Since all of these residues are located within the fourth repeat, the third repeat's stability must be less dependent on electrostatics. For the LZ_{GCN4} peptide used in our study the content of putatively destabilizing basic amino acid residues is 8 per 4 heptad repeats, thus making the sequence more sensitive to acidic pH. Indeed the estimated LZ_{GCN4} net charge at pH 7.1 is +1, while at pH 3.2 +8. This implies a feasibility of a coiled coil to the x-form transition being induced by these electrostatic repulsions. Interestingly most of the basic amino acid residues are located in the flanking regions of the LZ_{GCN4} sequence, with the central stretch of 16 residues containing only one, K18, in the middle (Figure 6A). Given distribution of positively charged residues coincides with the x-form ^1H-^{15}N NOEs and δC_α value patterns indicating a structured central core with two sites inclined to α helix.

Beyond the question of the x-form monomeric versus dimeric nature, is the issue of possible biological relevance of this conformation. The x-form population increases at low-peptide concentrations, which is relevant in vivo. On one hand favored by an acidic environment, on the other it is still detectable at neutral pH values. Although, the acidic buffering conditions may be considered as non-natural, one can expect a local pH decrease in the vicinity of nucleic acid polymers in the cell nucleus. Taking into account the presence of the x-form in GCN4 basic region−leucine zipper sequence (not only in isolated LZ domain), as well as the wide range of conditions where the x-form is populated, we propose that this structure is not just an off-pathway folding intermediate and not simply an unstructured monomer as in the case of LZ_{GCN4} fragments[36] or mutant sequences[38] but could be biologically relevant.

An attractive hypothesis to survey is the potential involvement of revealed LZ_{GCN4} x-conformation in the regulatory networks of bZIP and bHLH-LZ transcription factors. Common dimerization domains allow transcription factors in the LZ families to form a variety of homo- and heterodimers with different properties. Since these factors bind to promoter DNA in a sequence-specific manner, unique pairings of factors often results in unique pairings of DNA-binding preferences. Thus, by expressing different sets of subunits under different conditions, cells can generate complex regulatory circuits from a relatively small number of genes.[20] Accordingly, the larger the array of LZ transcription factors in a given genome, the greater the potential for complex transcriptional programs affecting the unique functions of individual cells, tissues, organs, and the species itself.[41] Plain monomer−dimer folding kinetics, taken together with tightness of interactions within the coiled coil interface, make it difficult to envision a mechanism allowing convenient and specific interchange of dimerization partners (and therefore transcriptional activities) within these regulatory networks. However, the existence of a stable intermediate conformation, can easily explain this phenomenon.

Besides the possible value of the x-form discovery for investigation of LZ transcription factors regulatory networks, new insights can also be gained in the direction of coiled coil folding studies. But what is more important, taking into account the multitude of cellular functions dependent on LZ transcription factors and other proteins bearing this motif, the equilibrium described in our study can be potentially employed as a model system in the development of various types of drugs, including antiviral and anticancer substances targeting the interaction interfaces within the LZ domains.[42−47]

Materials and Methods

Plasmid Constructions, Protein Expression and Purification. The LZ_{GCN4} peptide used in the current study has the following sequence: GLQRMKQLEDKVEELLSKNYHLENEVARLKKLVGER. This corresponds to the original and widely characterized GCN4-p1 peptide[16] with additional Gly-Leu-Gln N-terminal residues, two of those being GCN4 authentic residues, and Gly coming from the expression system.

The recombinant peptides were expressed in *Escherichia coli* BL21-(DE3) (Stratagene, La Jolla, CA) as fusions with bacteriophage λ-protein D[48] and released from the fusion using bovine enterokinase.[49]

The expression vector pHDe was constructed by cloning the bacteriophage λ-protein D gene (λcI857Sam7, Bohringer Mannheim, Germany) together with the downstream Gly-Ser linker and the enterokinase cleavage site (D_4K) into the pQE30 vector (Qiagen AG, Basel, Switzerland). DNA fragment coding for the leucine zipper GCN4 was amplified from pET3α-GCN4 plasmid (kindly provided by Dr. Christine Berger, University Zurich, Switzerland) and inserted into the pHDe vector via the SfoI/HindIII restriction sites downstream of the sequence encoding for the His_6-λpD-$(GS)(G_3S)_2$-(D_4K) construct. The identity of the final construct pHDe-LZgcn4 was confirmed by sequencing (Microsynth AG, Balgach, Switzerland).

For protein expression *Escherichia coli* BL21(DE3) cells (Stratagene, La Jolla, CA) were transformed with the pHDe-LZgcn4 vector following the instructions of the manufacturer. Freshly transformed cells were inoculated overnight in Spectra 9 medium (Spectra Stable Isotopes, MD) supplemented with BME vitamins solution (Sigma-Aldrich, Buchs, Switzerland). They were then diluted 1:20 with fresh medium and grown at 37 °C to a cell density $OD_{600} \approx 0.9$ before the expression was induced by the addition of isopropyl-β-D-thiogalactopyranoside (IPTG) to a final concentration of 1 mM. The cells were grown for a further 7−8 h, then harvested by centrifugation (5 min, 5000g), and frozen at −20 °C. For ^{15}N (^{15}N, ^{13}C)-labeled preparations Spectra 9 medium was supplied with $^{15}NH_4Cl$ (and ^{13}C−D-glucose) (Spectra Stable Isotopes, MD) as the sole source for nitrogen (and carbon).

Cell pellets were resuspended in Ni-NTA binding buffer $(NaCl)_{500}$-$(NaPi)_{20}$(imidazole)$_{50}$(7.4), disrupted in a French pressure cell at 11 000 psi (7.6×10^7 Pa) and centrifuged (45 min, 100000g) to separate the soluble fraction. His-tagged fusion protein was purified from the soluble fraction on a Ni-NTA metal-affinity column (Amersham-Pharmacia

(41) Deppmann, C. D.; Alvania, R. S.; Taparowsky, E. J. *Mol. Biol. Evol.* **2006**, *23*, 1480−92.
(42) Agou, F.; Courtois, G.; Chiaravalli, J.; Baleux, F.; Coic, Y. M.; Traincard, F.; Israel, A.; Veron, M. *J. Biol. Chem.* **2004**, *279*, 54248−57.
(43) Borges-Walmsley, M. I.; Beauchamp, J.; Kelly, S. M.; Jumel, K.; Candlish, D.; Harding, S. E.; Price, N. C.; Walmsley, A. R. *J. Biol. Chem.* **2003**, *278*, 12903−12.
(44) Berg, T.; Cohen, S. B.; Desharnais, J.; Sonderegger, C.; Maslyar, D. J.; Goldberg, J.; Boger, D. L.; Vogt, P. K. *Proc. Natl. Acad. Sci. U.S.A.* **2002**, *99*, 3830−5.
(45) Ahmad, A.; Yadav, S. P.; Asthana, N.; Mitra, K.; Srivastava, S. P.; Ghosh, J. K. *J. Biol. Chem.* **2006**, *281*, 22029−38.
(46) Kataoka, K.; Handa, H.; Nishizawa, M. *J. Biol. Chem.* **2001**, *276*, 34074−81.
(47) Surh, Y. J.; Kundu, J. K.; Na, H. K.; Lee, J. S. *J. Nutr.* **2005**, *135*, 2993S-3001S.
(48) Forrer, P.; Jaussi, R. *Gene* **1998**, *224*, 45−52.
(49) Liepnieks, J. J.; Light, A. *J. Biol. Chem.* **1979**, *254*, 1677−83.

Biotech, Uppsala, Sweden) according to the instruction of the manufacturer. Fractions containing the λpD-LZgcn4 fusion were dialyzed into enterokinase cleavage buffer $(Tris\text{-}HCl)_{20}(NaCl)_{50}(CaCl_2)_2(7.4)$ and subjected to enterokinase (Novagene, Darmstadt, Germany) cleavage for 24 h at room temperature at a concentration of $(fusion)_{0.5\ mg}(EK)_{7U}$-$(clevage\ buffer)_{1\ mL}$. After cleavage the 4.3 kDa LZgcn4 was separated from 15 kDa λpD by ultrafiltration on 5 kDa MWCO centrifugal filter devices (Millipore, Billerica, MA).

Final purification of the peptides was performed by reverse-phase HPLC on a C18 preparative column (Macherey-Nagel, Duren, Germany) using a water-acetonitrile gradient in the presence of 0.1% trifluoroacetic acid. Peptide identities were confirmed by MALDI-MS (FGCZ, Zurich, Switzerland). Peptide concentrations were determined from ^{1}H NMR spectra via integration of methyl-protons peak using L-Leucine (Sigma-Aldrich, Buchs, Switzerland) as a reference. Obtained values were consistent with the ones determined from absorbance at 280 nm (using extinction coefficient of the only Tyr20 tyrosine residue[50,51]).

NMR Spectroscopy. NMR experiments were performed at 37 °C on a Bruker AVANCE 600 MHz spectrometer equipped with a *z*-axis gradient triple resonance cryprobe and an AVANCE 900 MHz spectrometer. NMR data were processed with XWINNMR 3.2 (Bruker Biospin, Fallanden, Switzerland), analyzed using XEASY[52] and CARA (www.nmr.ch).[53] The ^{1}H chemical shifts were referenced to the DSS (sodium 2,2-dimethyl-2-silapentane-5-sulfonate) signal at 0 ppm, and ^{15}N and ^{13}C chemical shifts were referenced indirectly using the X/^{1}H gyromagnetic ratios.[54]

The concentration and pH dependencies of the x-form population were measured in 50 mM D_3-acetate, 40 mM KCl, pH 3.2. The pH of the samples was adjusted with potassium-D_3-acetate, and the exact values were measured at room-temperature both before and after the NMR experiments.

The assignments for the coiled coil conformation were obtained on the basis of the spectra recorded using 1 mM (monomer concentration) ^{15}N-^{13}C uniformly labeled LZ_{GCN4} peptide in 20 mM HEPES (2-[4-(2-hydroxyethyl)piperazin-1-yl]ethanesulfonic acid), 80 mM KCl, pH 7.1. The protein sample was further titrated down to the pH 3.2 and the changes in the chemical-shift values of assigned coiled coil residues were followed at each step of titration. The spectra for the x-form assignments were recorded using 0.25 mM LZ_{GCN4} peptide in 50 mM D_3-acetate, 40 mM KCl, pH 3.2. The same preparation was further used to obtain unfolded monomer reference sample, by diluting the peptide to 0.1 mM, adding urea to final concentration of 8 M, and adjusting the pH to 2.5 with hydrochloric acid.

Spin States in Conformationally Exchanging Molecules. For the mathematical treatment of the evolution of the density operator in the course of the reported NMR experiments, to extract quantitative information on the kinetic rates and populations from the spectra, several assumptions are made: (i) the molecule is in equilibrium between two spectroscopically distinct conformations A and A′ exchanging with a rate $k_{ex} = k_1 + k_{-1}$, which is slower than the frequency separation of the corresponding NMR resonances, for example, in slow exchange regime, a condition quantitatively defined by McConnel;[55] (ii) the chemical exchange should be a Markovian random process;[56] and (iii) the sudden jump approximation is assumed, which implies that the magnetization does not change orientation during the chemical exchange.[56] A product space between chemical configuration space and magnetization, a composite superspace, is required to account for the flow of magnetization during the chemical exchange[56,57] as it is implemented as a homogeneous version of the stochastic Liouvillian equations[58] in the NMR simulation program QSIM.[59]

To simplify product operator description of the reported NMR experiments we further assume that the spin-state operators are mixed either in the rotating frame under conditions of spin locking[60] achieved by windowless sequences of composite rf-pulses[61] or in the longitudinal direction, where only the operators representing magnetization modes[62] should be considered.[26] Under these assumptions only transverse and longitudinal subspaces of the composite superspace defined by the corresponding spin-state operators contributing to the detectable signal can be considered. The present discussion is restricted to two exchanging two-spin-$^1/_2$ systems, *IS* and *I′S′*, where *I* and *I′* stand for a proton and *S* and *S′* for a heteronuclear spin (e.g., ^{15}N or ^{13}C), coupled via a scalar coupling constant J_{IS}. This situation represents one of the most common spin systems encountered, e.g., for backbone HN or HC^{α} moieties. The conformation exchange process and longitudinal relaxation of ^{1}H (owing to the bulk of protons in protein), result into effective mapping of initial spin states entering the mixing period on the spin states subsequently detected as a signal given by

$$S_i^{\alpha} \rightarrow S'^{\alpha}_i \tag{1.1}$$

$$S_i^{\alpha} \rightarrow S'^{\beta}_i \tag{1.2}$$

In eq 1, the single transition basis operators $S_i^{\alpha} = {}^1/_2 S_i + S_i I_z$ and $S_i^{\beta} = {}^1/_2 S_i - S_i I_z$ are used, where *i* stands for "z", "+" or "−". For sufficiently short mixing periods, the buildup of the target operators is monoexponential with the corresponding buildup rates of k_{ex} and $1/(2T_{1Hbulk})$, respectively.[32] The mapping given by eq 1.1 represents the productive magnetization transfer pathway, which is selected in the NMR experiments, while the spurious transfer of eq 1.2 should be suppressed.

Spin State Exchange in the Rotating Frame. In the slow-exchange regime with the strength of the locking rf-field ω_{rf} satisfying the condition $\omega_{S,rf} \gg |\Omega_S - \Omega'_S|$, where Ω_S is the chemical shift relative to the carrier frequency of the spin *S*, the transfer of the ^{1}H spin-state selective ^{15}N coherence due to the exchange can be described by eq 1. For the 4(1)D XYEX-TROSY experiment of Figure 3, two equivalent (in terms of coherent evolution of the density operator) magnetization transfer pathways are given by

$$I_z^{\alpha} + S_z^{\alpha} \rightarrow I_+ S_- \exp[i(\Omega_I - \Omega_S)t_1] \rightarrow S_-^{\beta} \rightarrow S'^{\beta}_- \exp[i(-\Omega'^{\beta}_S)t_2] \rightarrow I_-^{\alpha} \exp[i(-\Omega'^{\alpha}_I)t_3] \tag{2.1}$$

$$I_z^{\beta} - S_z^{\beta} \rightarrow I_+ S_+ \exp[i(\Omega_I + \Omega_S)t_1] \rightarrow S_+^{\alpha} \rightarrow S'^{\alpha}_+ \exp[i(\Omega'^{\alpha}_S)t_2] \rightarrow I_-^{\beta} \exp[i(-\Omega'^{\beta}_I)t_3] \tag{2.2}$$

where $\Omega_i^{\alpha} = \Omega_i + \pi J_{IS}$, $\Omega_i^{\beta} = \Omega_i - \pi J_{IS}$, and $i = I$ or *S*. The initial steady-state I_z and S_z polarizations are the sum of the corresponding single-transition polarization operators, which can be considered separately.[29] It should be noted that the pathway 1 is optimized in terms of transverse relaxation and is enhanced by the steady-state magnetization of the spin *S*.[30] Three- and four- spin-$^1/_2$ systems I_2S and I_3S found in methylene and methyl groups do not result in detectable ^{1}H signal, and therefore the corresponding magnetization transfer pathways are not explicitly described.

The echo−anti-echo type Fourier transform in all spectral dimensions of the interferograms acquired with two executions of the pulse

(50) Edelhoch, H. *Biochemistry* **1967**, *6*, 1948−54.
(51) Gill, S. C.; von Hippel, P. H. *Anal. Biochem.* **1989**, *182*, 319−26.
(52) Bartels, C.; Xia, T. H.; Billeter, M.; Guntert, P.; Wuthrich, K. *J. Biomol. NMR* **1995**, *6*, 1−10.
(53) Keller, R. L. J. *The Computer Aided Resonance Assignment Tutorial*, 1st ed.; Cantina Verlag: Germany, 2004.
(54) Wishart, D. S.; Bigam, C. G.; Yao, J.; Abildgaard, F.; Dyson, H. J.; Oldfield, E.; Markley, J. L.; Sykes, B. D. *J. Biomol. NMR* **1995**, *6*, 135−40.
(55) McConnell, H. M. *J. Chem. Phys.* **1958**, *28*, 430−31.
(56) Jeener, J. *Adv. Magn. Reson.* **1982**, *10*, 1−51.
(57) Kühne, R. O.; Schaffhauser, T.; Wokaun, A.; Ernst, R. R. *J. Magn. Reson.* **1979**, *35*, 39−67.
(58) Helgstrand, M.; Hard, T.; Allard, P. *J. Biomol. NMR* **2000**, *18*, 49−63.
(59) Helgstrand, M.; Allard, P. *J. Biomol. NMR* **2004**, *30*, 71−80.
(60) Deverell, C.; Morgan, R. E.; Strange, J. H. *Mol. Phys.* **1970**, *18*, 553−59.
(61) Bai, N. S.; Ramachandran, R. *J. Magn. Reson., Ser. A* **1993**, *105*, 298−303.
(62) Canet, D. *Prog. Nucl. Magn. Reson. Spectrosc.* **1989**, *21*, 237−91.

sequence of Figure 3 results in two spectra, S_{ZQ+DQ} and S_{ZQ-DQ}, representing the sum and difference of signals described by eq 2.1 and 2.2. The extraction of the signal corresponding to the individual pathways is achieved by subsequent adding or subtracting of S_{ZQ+DQ} and S_{ZQ-DQ} spectra. The suppression of the spurious pathway of eq 1.2 can be achieved by incorporation of the relaxation compensation element in the middle of the mixing period.[63] Alternatively, the spurious cross-peaks in the S_{ZQ} subspectrum resulting from the cross-talk of eq 1.2 can be, to a very good extent, eliminated by subtracting S_{DQ} spectrum shifted in ω_2 and ω_3 dimensions by J_{IS} Hz and multiplied with an empirically weighed factor typically in the range of 0.1. The latter technique we preferred in the current study, since it does not require interruption of the supercycle of the spin-locking pulse train and incorporation of an extra delay of $^1/_2J_{IS}$ in the mixing period during which no polarization transfer due to the exchange occurs.

Spin State Exchange in Longitudinal Direction. In the case of slow exchange rates, mixing of the magnetization modes[26,62] instead of spin-selective coherences can be considered owing to the longer corresponding relaxation rates and lack of need to decouple passive *J* couplings. With the cost of decreasing sensitivity by a factor of 2, the experimental scheme of Figure 3 can be modified in such a way, that the transfer $S_-^\beta \rightarrow S'^{\beta}_-$ is achieved in two steps implemented in two separate experiments (see ZEX-TROSY of Figure S3, Supporting Information). At first in $S_-^\beta = S_x^\beta - iS_y^\beta$, S_x^β is converted to S_z^β and subsequently mixed with $S_z'^\beta$, which is, in turn, followed by a conversion to $S_x'^\beta$. This pathway is complemented with the corresponding transfer of S_y^β. The complete pathways of eq 1 is reconstructed by addition of thus acquired two subspectra followed by the transformation procedure described earlier.

Spin State Exchange in the Doubly Rotating Frame. Two asynchronously rotating coordinate frames where the *I* and *S* spins are locked with windowless composite pulse sequences satisfying the conditions $\omega_{S,rf} \gg |\Omega_S - \Omega'_S|$ and $\omega_{I,rf} \gg |\Omega_I - \Omega'_I|$ can be used to reduce the total duration of polarization transfer periods by $1/J_{IS}$ comparing to XYEX-TROSY of Figure 3 and still obtain a fully sensitivity-enhanced spin-state exchange pseudo-4D experiment. For the 4(1)D (XY)2EX-TROSY experiment of Figure S1 (Supporting Information), two equivalent magnetization transfer pathways are given by

$$I_z^\alpha + S_z^\alpha \rightarrow I_+S_- \exp[i(\Omega_I - \Omega_S)t_1] \rightarrow I'_+S'_- \rightarrow I'_+S'_- \exp[i(-\Omega'_S)t_2] \rightarrow I_-^\alpha \exp[i(-\Omega'^{\alpha}_I)t_3] \quad (3.1)$$

$$I_z^\beta - S_z^\beta \rightarrow I_+S_+ \exp[i(\Omega_I + \Omega_S)t_1] \rightarrow I'_+S'_+ \rightarrow I'_+S'_+ \exp[i(\Omega'_S)t_2] \rightarrow I_-^\beta \exp[i(-\Omega'^{\beta}_I)t_3] \quad (3.2)$$

Note that the spurious magnetization transfer owing to proton−proton dipolar relaxation mechanisms does not occur, and thus there is no need for compensation of spurious cross-peaks in the spectra. The advantage of the ZQ/DQ version is the absence of the delays in the middle polarization transfer element, which might result in potential improvement in sensitivity. The passive coupling constants $J_{H\alpha HN}$ and $J_{H\beta HN}$ do not contribute to the signal dephasing during mixing because of the selection of relatively low rf-power to lock $^1H^N$ magnetization thus resulting in effective decoupling of $^1H^N$ spins from all other protons. However we have not achieved the maximum sensitivity with this scheme possibly because of the loss of coherences to imperfections of rf-pulses during mixing (data not shown). However, this might be improved with further optimization of mixing sequences.

Acknowledgment. This work is financially supported by grants from the Roche Research Foundation (to Y.N.) and the NTU (to K.P.).

Supporting Information Available: Figures S1, S2, S3: scheme of 4(1)D (XY)2EX-TROSY experiment; scheme of 4(1)D PFG-XYEX-TROSY experiment; scheme of 4(1)D PFG-ZEX-TROSY experiment. Listings S1 and S2: Bruker Avance pulse program for 4(1)D XYEX-TROSY experiment; Bruker Avance pulse program for 4(1)D (XY)2EX-TROSY experiment. This material is available free of charge via the Internet at http://pubs.acs.org.

JA0685295

(63) Loria, J. P.; Rance, M.; Palmer, A. G. *J. Am. Chem. Soc.* **1999**, *121*, 2331−2.
(64) Cavanagh, J.; Palmer, A. G.; Wright, P. E.; Rance, M. *J. Magn. Reson.* **1991**, *91*, 429−36.